Performance Evaluation of Spectrum Sensing Using Recovered Secondary Frames With Decoding Errors

Liang Tang, *Student Member, IEEE,* Yunfei Chen, *Senior Member, IEEE,*
Arumugam Nallanathan, *Senior Member, IEEE*, and Evor L. Hines

***Abstract*—The performance of spectrum sensing using the recovered secondary frames is analyzed. Unlike the previous work that assumes perfect decoding of the secondary signal, the new analysis takes the decoding errors into account and therefore provides a more realistic comparison between the new model and the conventional model. Both the receiver operating characteristics curves for spectrum sensing and the achievable throughput for data transmission are derived. Effects of fading and error control codes are also investigated. Numerical results show that the new model that considers the decoding error outperforms the conventional model when the number of transmitted secondary frames is below a certain threshold. An upper bound performance can also be obtained by ignoring the decoding error. The threshold is determined by the primary user traffic, the spectrum sensing technique and the secondary signal modulation scheme.**

***Index Terms*—Achievable throughput, cognitive radio, spectrum sensing.**

I. Introduction

COGNITIVE radio has been proposed as a promising solution to the spectrum scarcity problem caused by the conflict between spectrum congestion and spectrum underutilization [1]. It provides the secondary users (SU) with opportunistic access to the licensed bands through identifying the unoccupied spectrum holes. By allowing this opportunistic access, a better spectrum utilization can be achieved [2]. However, this opportunistic access also leads to possible degradation in the primary user (PU)'s service quality due to the possible interference from the SUs. It is therefore a crucial requirement for the SUs to correctly identify the PU's existence to minimize this interference [3]. This is achieved through spectrum sensing. Commonly used spectrum sensing methods include matched-filtering detection, energy detection, cyclostationary detection and feature detection [4].

In the draft IEEE 802.22 standard [5], a frame structure is adopted which allows the SU to perform spectrum sensing periodically. In this structure, the entire secondary link time is divided into multiple consecutive frames. Each frame consists of a sensing period and a transmission period. During the sensing period or the "quiet" period, the SUs stop all their transmissions and perform spectrum sensing in the licensed channel. At the end of the "quiet" period, if the channel is considered to be idle, the SUs carry out their transmission in the following transmission period. Otherwise, they will wait until the next frame arrives to sense the channel again in the "quiet" period before any secondary usage. In the rest of this paper, this structure is referred to as the conventional model. In the conventional model, more sensing time means less transmission time for a fixed frame length. Thus, there exists an optimal sensing time that maximizes the achievable throughput [6], [7]. Adaptive scheduling of this optimal sensing time has been studied in [7].

To increase the achievable throughput further, in [8] a new model was proposed. In this model, the entire secondary link time is still divided into multiple consecutive frames. The initial sensing is performed in the "quiet" periods of the first several conventional secondary frames until the idle status of the channel is identified or acquired. In the following frames, the whole secondary frame is devoted for data transmission without any dedicated sensing or "quiet" period. The following sensing is only performed by using the recovered received secondary frames after the SU signal is decoded and removed from the received secondary frame at the SU receiver.

This model has several advantages over the conventional model. First, by using the whole secondary frame for sensing to track the status of the channel after it is initially detected free, the sensing time increases and therefore, the sensing accuracy improves. This is especially important for feature detection where a long sensing time is normally required. Second, by using the whole secondary frame for transmission, the achievable throughput of the SU is maximized. Third, the calculation of the optimal sensing time for each frame is no longer required as the secondary frame does not have any dedicated sensing period and only the recovered secondary frame is used for sensing. The main disadvantage of this new model is that in reality, the recovered received secondary frames used in the following sensing may be corrupted by the SU signals due to decoding errors. This reduces the sensing accuracy. In [8], it was assumed that the SU signal can always be correctly decoded and be completely removed from the received secondary frame. Therefore, the new model always benefits from a longer sensing time.

In reality, decoding errors may occur such that the SU signal will not be completely removed. In this case, the sensing accuracy based on the recovered received secondary frame

Manuscript received September 30, 2011; revised March 10 and May 5, 2012; accepted May 7, 2012. The associate editor coordinating the review of this paper and approving it for publication was M. McKay.

L. Tang, Y. Chen, E. L. Hines are with the School of Engineering, University of Warwick, Coventry, CV4 7AL, UK (e-mail: {liang.tang, yunfei.chen, e.l.hines}@warwick.ac.uk).

A. Nallanathan is with the Centre for Telecommunications Research, School of Natural and Mathematical Sciences, Kings College London, London, WC2R 2LS, UK (e-mail: nallanathan@ieee.org).

Digital Object Identifier 10.1109/TWC.2012.060212.111800

will be reduced by the decoding error. The reduced sensing accuracy will consequently degrade the SU data transmission in the next frame due to possible interferences from the PU that has been missed. This causes even larger decoding error. Eventually, the afore-mentioned advantage of the new model may be compromised by the accumulated errors. Hence, in reality, the results in [8] only provided an ideal upper bound of the system performance. Furthermore, the system performance in [8] was analyzed for only one single frame by assuming a constant occupancy status of the PU. However, even when there is no decoding error, the data transmission suffers from the sensing error based on the previous frame. This effect does not occur when only a single frame is considered. As well, the PU may change its occupancy status throughout the multiple frames. A more comprehensive investigation that considers the decoding error and multiple consecutive frames with PU traffic is crucial in deploying the new model. It is therefore of great interest to investigate whether this new model can outperform the conventional model or when the advantages will outplay the disadvantages in more realistic situations.

In this paper, the performance of the new model proposed in [8] is further developed to contain multiple consecutive frames and is analyzed by taking into account the decoding errors with PU traffic to give a more comprehensive comparison between the conventional model and the new model. The effects of different types of SU modulation schemes and different sensing techniques are also studied. In order to fully examine the new model, the effects of fading and error control codes (ECC) are also investigated. Numerical results show that, while the new model benefits from the longer sensing period and the longer transmission period by using the whole secondary frame for data transmission and the whole recovered secondary frame for spectrum sensing in the tracking phase, respectively, as the number of transmitted secondary frames increases, the new model will lose its advantages and eventually underperform the conventional model due to the accumulated errors from spectrum sensing and decoding. Thus, there exists a threshold for the number of the transmitted secondary frames in the new model below which it outperforms the conventional model. This threshold is affected by the spectrum sensing technique as well as the SU signal modulation scheme.

II. System Model

Consider a cognitive radio network with two types of users operating in the same licensed channel: a PU that has the right to access the channel at any time and a SU that accesses the channel on an opportunistic basis. The secondary link operates on a frame-by-frame basis, with N consecutive frames each of which has a frame duration of T. Throughout the N frames, the occupancy status of the PU may change depending on the primary traffic, which is defined by the PU channel holding time. Several channel holding time distributions have been proposed for legacy systems in the literature, such as exponential [9] [10], log-normal [11] [12], Gamma [13] [14] and Erlang distributions [15]. The probability that the PU changes its occupancy status during the n^{th} frame is expressed using the probability mass function (PMF) of the channel holding time as [16]

$$p_{\lambda(n)} = F(nT) - F\big((n-1)T\big), \tag{1}$$

where $F(t)$ is the cumulative distribution function (CDF) of the channel holding time and $n = 1, 2, ...N$ is the frame index. Assume that the PU has an exponential holding time with mean parameter λ [10], as it is the most commonly used channel holding time distribution model and cognitive radio aims to reuse their bands. Then, $F(t)$ can be expressed as $F(t) = 1 - e^{-\lambda t}$. Other distributions can be examined in a similar way. It is further assumed that the PU does not change its occupancy status during each secondary frame. This is assumed for both the conventional model and the new model to provide a fair comparison between these two models. It is also the case when the secondary frame is short or when the primary user traffic is low (long holding time), similar to the assumption in [7], [8], [10]. An extension to the case when the PU arrives or leaves during each secondary frame is very difficult and will be a topic for future research.

A. Conventional model

In the conventional model, each frame is divided into a sensing period τ and a transmission period $T-\tau$. The sensing period acts as a "quiet" period from the SU's point of view, as during the sensing period the SU data transmission is stopped. The received signal at the SU receiver during the sensing period of the n^{th} frame is sampled at a rate of f_s. The samples used for spectrum sensing can be expressed as

$$Y_{con,i(n)} = a s_{p,i} + w_i \tag{2}$$

where $i = 1, 2, \ldots\ldots \tau f_s$, is the sample index, $a = 0, 1$ represents the status of the PU with 0 being absent and 1 being present, $s_{p,i}$ denotes the received PU signal sample and w_i is the additive white Gaussian noise sample. If energy detection is used for spectrum sensing, the sensing process becomes a binary hypothesis test problem as

$$y_{con(n)} = \begin{cases} \sum_{i=1}^{\tau f_s} w_i^2, & H_0, \\ \sum_{i=1}^{\tau f_s} (s_{p,i} + w_i)^2, & H_1 \end{cases} \tag{3}$$

where H_0 represents the hypothesis that the PU is absent hence the channel is idle, and H_1 represents the hypothesis that the PU is present hence the channel is busy.

Two probabilities are useful in sensing: the probability of false alarm, defined as the probability that the SU falsely considers the PU to be present while it is actually absent, and the probability of detection, defined as the probability that the presence of the PU is correctly identified by the SU. In the conventional model using energy detection, the probability of detection and the probability of false alarm of the n^{th} frame can be obtained as [17]

$$P_{d_{conED}(n)}(\tau) = \frac{1}{2} erfc\left(\frac{\eta_{con_{ED}(n)} - \tau f_s \gamma_p - \tau f_s}{2\sqrt{2\tau f_s \gamma_p + \tau f_s}}\right) \tag{4}$$

and

$$P_{f_{conED}(n)}(\tau) = \frac{1}{2} erfc\left(\frac{\eta_{con_{ED}(n)} - \tau f_s}{2\sqrt{\tau f_s}}\right) \tag{5}$$

respectively, where $\eta_{con_{ED}(n)}$ is the decision threshold for the conventional model using energy detection and γ_p is the received PU SNR.

At the end of the "quiet" period, there are two scenarios where the SU transmission will start: the sensing correctly identifies the absence of the PU, or the sensing mis-detects the presence of the PU [6]. In the conventional model, the occurring probabilities of these two scenarios can be expressed as $P_{H_{0_{con}}(n)}\left(1-P_{f_{conED}(n)}(\tau)\right)$ and $P_{H_{1_{con}}(n)}\left(1-P_{d_{conED}(n)}(\tau)\right)$, respectively, where $P_{H_{0_{con}}(n)}$ and $P_{H_{1_{con}}(n)}$ are the probabilities that the PU is absent or present at the beginning of the n^{th} frame, respectively. They can be derived as

$$P_{H_{0_{con}}(n)} = P_{H_{0_{con}}(n-1)}\left(1-p_{\lambda(n)}\right)+P_{H_{1_{con}}(n-1)}p_{\lambda(n)} \quad (6)$$

and

$$P_{H_{1_{con}}(n)} = P_{H_{0_{con}}(n-1)}p_{\lambda(n)}+P_{H_{1_{con}}(n-1)}\left(1-p_{\lambda(n)}\right) \quad (7)$$

where $p_{\lambda(n)}$ is given in (1), and $P_{H_{0_{con}}(0)}$ and $P_{H_{1_{con}}(0)}$ are the *a priori* probabilities of the two hypotheses for $n = 0$, respectively .

Define γ_s as the SU SNR. The channel capacity can be expressed as $C_0 = \log_2(1+\gamma_s)$ and $C_1 = \log_2\left(1+\frac{\gamma_s}{1+\gamma_p}\right)$ for the cases when the PU is absent or present, respectively. The total throughput of the N consecutive frames can be obtained as

$$\begin{aligned} R_{con_{ED}}(\tau) = \sum_{n=1}^{N} \Big(& P_{H_{0_{con}}(n)}\left(1-P_{f_{conED}(n)}(\tau)\right)C_0 \\ & +P_{H_{1_{con}}(n)}\left(1-P_{d_{conED}(n)}(\tau)\right)C_1\Big)\frac{T-\tau}{T}. \end{aligned} \quad (8)$$

In the above equation, the term $\frac{T-\tau}{T}$ reflects the penalty on the SU data transmission due to the "quiet" period used for the spectrum sensing in each frame of the conventional model.

The above analysis applies to energy detection. One can also derive it for feature detection [18]. Assume that the received PU samples are Gaussian with mean zero and correlation $\rho^{|i-j|}$, where ρ is a constant and $|i-j|$ is the sample time difference. Define the sample auto-correlation of the received signal in the conventional model as

$$\theta_{con}(l) = \frac{1}{\tau f_s}\sum_{i=1}^{\tau f_s-1} Y_{con,i}Y_{con,i-l}, \qquad l = 1, ..., L-1 \quad (9)$$

where $Y_{con,i}$ is the i^{th} received sample and L is the smoothing factor.

The sample correlation matrix of the received signal is then expressed as [19]

$$A_{Y_{con}} = \begin{pmatrix} \theta_{con}(0) & \theta_{con}(1) & \dots & \theta_{con}(L-1) \\ \theta_{con}(1) & \theta_{con}(0) & \dots & \theta_{con}(L-2) \\ \vdots & \vdots & \vdots & \vdots \\ \theta_{con}(L-1) & \theta_{con}(L-2) & \dots & \theta_{con}(0) \end{pmatrix}. \quad (10)$$

If the maximum-eigenvalue detector is used in this case, the probability of detection and the probability of false alarm can be derived as [20]

$$P_{d_{conME}(n)}(\tau) = 1 - TW_1\left(\frac{\eta_{con_{ME}(n)}\tau f_s - \frac{\tau f_s \vartheta_{max}}{\sigma_w^2} - \mu_{con}}{\upsilon_{con}}\right) \quad (11)$$

and

$$P_{f_{conME}(n)}(\tau) = 1 - TW_1\left(\frac{\eta_{con_{ME}(n)}\tau f_s - \mu_{con}}{\upsilon_{con}}\right) \quad (12)$$

respectively, where $TW_1(\cdot)$ is the Tracy-Widom distribution of order 1, $\eta_{con_{ME}(n)}$ is the decision threshold for the maximum-eigenvalue detector in the conventional model, ϑ_{max} is the maximum eigenvalue of the statistical correlation matrix of the PU signal, σ_w^2 is the noise variance, $\mu_{con} = \left(\sqrt{\tau f_s - 1}+\sqrt{L}\right)^2$ and $\upsilon_{con} = \left(\sqrt{\tau f_s - 1}+\sqrt{L}\right)\left(\frac{1}{\sqrt{\tau f_s - 1}}+\frac{1}{\sqrt{L}}\right)$.

Hence, for a pair of target probabilities $P_{d_{conME}(n)}(\tau) = P_d^{'}$ and $P_{f_{conME}(n)}(\tau) = P_f^{'}$, the minimum number of samples required at spectrum sensing can be derived from (11) and (12) as

$$M_{con_{ME}(n)} = \frac{\upsilon_{con}\sigma_w^2}{\vartheta_{max}}\left(TW^{-1}(1-P_f^{'}) - TW^{-1}(1-P_d^{'})\right). \quad (13)$$

If covariance-based detector is applied in the conventional model during the spectrum sensing, the probability of detection and the probability of false alarm can be derived as

$$P_{d_{conCOV}(n)}(\tau) = 1 - Q\left(\frac{\frac{1}{\eta_{con_{COV}(n)}} + \frac{\alpha_L\gamma_p}{\eta_{con_{COV}(n)}(\gamma_p+1)} - 1}{\sqrt{\frac{2}{\tau f_s}}}\right) \quad (14)$$

and

$$P_{f_{conCOV}(n)}(\tau) = 1 - Q\left(\frac{\frac{1}{\eta_{con_{COV}(n)}}\left(1+(L-1)\sqrt{\frac{2}{\tau f_s \pi}}\right) - 1}{\sqrt{\frac{2}{\tau f_s}}}\right) \quad (15)$$

respectively, where $Q(t) = \frac{1}{\sqrt{2\pi}}\int_t^{\infty} e^{-u^2/2}du$, $\eta_{con_{COV}(n)}$ is the decision threshold for the covariance-based detector and $\alpha_L = \frac{2}{L}\sum_{l=1}^{L-1}(L-l)|E\left[s_{p,i}s_{p,i-l}\right]/E\left[s_p^2\right]|$ with $E\left[s_p^2\right]$ being the PU signal power. Hence, for a pair of target probabilities $P_{d_{conCOV}(n)}(\tau) = P_d^{'}$ and $P_{f_{conCOV}(n)}(\tau) = P_f^{'}$ using the covariance-based detector, the minimum number of samples required to achieve these targets in this case can be derived from (14) and (15) as

$$\begin{aligned} M_{con_{COV}(n)} = 2\Big(\frac{\gamma_p+1}{\alpha_L\gamma_p}\Big(Q^{-1}(1-P_d^{'})(1+\frac{L-1}{\sqrt{\pi}}) \\ -Q^{-1}(1-P_f^{'})(1+\frac{\alpha_L\gamma_p}{\gamma_p+1})+\frac{L-1}{\sqrt{\pi}}\Big)\Big)^2. \end{aligned} \quad (16)$$

The achievable throughput of the conventional model using feature detection can also be derived by using same method as (6) - (8), but replacing the probability of detection and the probability of false alarm with (11) and (12) for the maximum-eigenvalue detection and with (14) and (15) for the covariance-based detection.

B. Ideal upper bound of the new model

In the new model, after an initial spectrum sensing that acquires the idle status of the licensed channel, the SU carries out data transmission for the entire duration of T in the following secondary frames. At the SU receiver, the SU signal is decoded and deducted from the received secondary frame. The recovered received secondary frame is then used for spectrum sensing. At the end of spectrum sensing, the SU stops data transmission in the next frame if spectrum sensing considers the PU to be present. Otherwise, the SU transmission continues in the next frame [8]. In this model, both spectrum sensing and data transmission are performed using the entire frame duration of T after the licensed channel is acquired. Then, the received secondary frame at the secondary receiver in the n^{th} frame can be expressed as

$$Y_{ide,j(n)} = as_{p,j} + s_{s,j} + w_j \tag{17}$$

where $j = 1, 2, \ldots\ldots Tf_s$, is the sample index, $s_{s,j}$ is the sample of the secondary signal and all the other symbols are defined as before.

Ideally, as was assumed in [8], the decoding process for the received secondary frame is error-free. The SU signal can then be completely removed from the received signal in (17). The recovered received secondary frame used for the spectrum sensing becomes exactly the same as (2) in the conventional model, only with an increased number of samples due to the whole frame being used for sensing. Therefore, when energy detection is applied, the probability of detection and the probability of false alarm in the n^{th} frame for the ideal case of the new model can be obtained by replacing τ in (4) and (5) with T to give

$$P_{d_{ideED}(n)}(T) = \frac{1}{2} erfc\left(\frac{\eta_{ide_{ED}(n)} - Tf_s\gamma_p - Tf_s}{2\sqrt{2Tf_s\gamma_p + Tf_s}}\right) \tag{18}$$

and

$$P_{f_{ideED}(n)}(T) = \frac{1}{2} erfc\left(\frac{\eta_{ide_{ED}(n)} - Tf_s}{2\sqrt{Tf_s}}\right) \tag{19}$$

respectively, where $\eta_{ide_{ED}(n)}$ is the decision threshold in this case. One sees that sensing in the ideal case of the new model has larger probability of detection or smaller probability of false alarm than those in the conventional model, as $T > \tau$ [8].

Also, in this case, the n^{th} frame can only be used for data transmission if spectrum sensing in the $(n-1)^{th}$ frame mis-detects the PU's existence or correctly identifies the PU's absence. Therefore, the probability that the PU is actually absent at the end of the $(n-1)^{th}$ frame and is correctly identified so that the n^{th} frame can be used for data transmission is derived as

$$\begin{aligned} P_{H_{0_{ide}}(n)} = {} & P_{H_{0_{ide}}(n-1)}\left(1 - P_{f_{ideED}(n)}(T)\right)\left(1 - p_{\lambda(n)}\right) \\ & + P_{H_{1_{ide}}(n-1)}\left(1 - P_{d_{ideED}(n)}(T)\right) p_{\lambda(n)} \end{aligned} \tag{20}$$

and the probability that the PU is present at the end of the $(n-1)^{th}$ frame and is mis-detected so that the n^{th} frame is used for data transmission is derived as

$$\begin{aligned} P_{H_{1_{ide}}(n)} = {} & P_{H_{0_{ide}}(n-1)}\left(1 - P_{f_{ideED}(n)}(T)\right) p_{\lambda(n)} + \\ & P_{H_{1_{ide}}(n-1)}\left(1 - P_{d_{ideED}(n)}(T)\right)\left(1 - p_{\lambda(n)}\right). \end{aligned} \tag{21}$$

Since data transmission in the new model is carried out for the entire frame duration of T, the transmission process does not suffer from the penalty caused by the "quiet" period, as in the conventional model. Thus, the total achievable throughput of the N frames for the ideal case is

$$R_{ide_{ED}} = \sum_{n=1}^{N}\left(P_{H_{0_{ide}}(n)}C_0 + P_{H_{1_{ide}}(n)}C_1\right). \tag{22}$$

When feature detection is applied for spectrum sensing, the probability of detection and the probability of false alarm can be obtained by replacing τf_s with Tf_s in (11) and (12) for the maximum-eigenvalue detector, and in (14) and (15) for the covariance-based detector. The achievable throughput can then be derived by using (20) - (22) with the new probabilities of detection and false alarm. Note that [8] only gives the results of the n^{th} frame in (18) and (19), which ignores the fact that the sensing performance from the $(n-1)^{th}$ frame will affect that of the n^{th} frame while our analysis considers this fact in (20) and (21) .

III. Realistic Analysis of the New Model

In reality, the decoding process for the received secondary frame in the new model is not ideal. Consequently, the SU signal may not always be correctly decoded and be completely removed from the received secondary frame. The sensing accuracy will therefore be adversely affected when the recovered received secondary frame is used for spectrum sensing. This further degrades the performance of the new model. Moreover, neighboring frames will affect each other and all the frames will be affected by the PU traffic. In the following, we start with the decoding process. Based on the imperfect decoding, we will derive the probabilities of detection and false alarm for spectrum sensing while considering multiple frames with PU traffic. Since spectrum sensing is performed after detection and accurate channel estimates are needed for detection, perfect channel state information (CSI) is assumed for spectrum sensing. Moreover, channel estimation with active PU traffic is a new topic that needs to be considered by secondary detection not spectrum sensing, and channel estimation coupled with spectrum sensing is beyond the scope of this paper.

A. Decoding

Consider binary phase shift keying (BPSK) for the SU signal. The received secondary frame at the SU receiver in the n^{th} frame can be expressed as

$$Y_{new,j(n)} = as_{p,j} + s_{s,j} + w_j \tag{23}$$

where $s_{s,j}$ is the SU signal with $s_{s,j} = -\sqrt{\epsilon_b}$ or $s_{s,j} = +\sqrt{\epsilon_b}$, and ϵ_b is the bit energy of the SU signal. Note that the SU is assumed to be corrupted by additive white Gaussian noise (AWGN) only and there is only one bit per symbol in BPSK.

The received secondary frame at the SU receiver is decoded. Denote the total number of transmitted SU symbols as x. The symbol duration of each SU signal symbol is $t_s = \frac{T}{x}$. Denote the *a priori* probabilities of a $-\sqrt{\epsilon_b}$ and a $+\sqrt{\epsilon_b}$ being transmitted as $P_{(-\sqrt{\epsilon_b})}$ and $P_{(+\sqrt{\epsilon_b})}$, respectively. When the PU is absent from the licensed channel, the received secondary frame contains only the SU signal and noise. Thus, (23) can

be simplified as $Y_{new,j(n)} = s_{s,j} + w_j$. In this case, the symbol error rate of each SU symbol given that a $-\sqrt{\epsilon_b}$ or a $+\sqrt{\epsilon_b}$ is transmitted can be expressed as

$$\begin{aligned} B_{H_0} &= B_{H_0(-\sqrt{\epsilon_b})} = B_{H_0(+\sqrt{\epsilon_b})} \\ &= P\left(-\sqrt{\epsilon_b}|H_0\right) = P\left(+\sqrt{\epsilon_b}|H_0\right) = Q\left(\sqrt{2\gamma_s}\right). \end{aligned} \tag{24}$$

Assume that out of the x transmitted symbols, q_0 symbols are $-\sqrt{\epsilon_b}$ and g_0 of the q_0 symbols are incorrectly decoded as $+\sqrt{\epsilon_b}$. Similarly, assume that k_0 symbols out of the $x - q_0$ transmitted $+\sqrt{\epsilon_b}$ are incorrectly decoded as $-\sqrt{\epsilon_b}$. Thus, for a duration of $(g_0 + k_0)t_s$, the SU signal is not removed from the received secondary frame, whilst for a duration of $(x - g_0 - k_0)t_s$, the SU signal is correctly decoded and completely removed. Thus, when PU is absent, the conditional probability of occurring for this case can be derived as

$$\begin{aligned} p(x, q_0, g_0, k_0|H_0) &= \left(P_{(-\sqrt{\epsilon_b})}B_{H_0}\right)^{g_0} \\ &\left(P_{(-\sqrt{\epsilon_b})}\left(1 - B_{H_0}\right)\right)^{q_0 - g_0}\left(P_{(+\sqrt{\epsilon_b})}B_{H_0}\right)^{k_0} \\ &\left(P_{(+\sqrt{\epsilon_b})}\left(1 - B_{H_0}\right)\right)^{x - q_0 - k_0} \end{aligned} \tag{25}$$

where independent symbols are assumed.

On the other hand, when the PU is present in the licensed channel but is missed by the SU in the $(n-1)^{th}$ frame, the data transmission is still carried out in the n^{th} frame. During the decoding process, the PU acts as an interference to the SU signal, and the symbol error rate of each SU symbol given that a $-\sqrt{\epsilon_b}$ or a $+\sqrt{\epsilon_b}$ is transmitted can be derived as

$$\begin{aligned} B_{H_1} &= B_{H_1(-\sqrt{\epsilon_b})} = B_{H_1(+\sqrt{\epsilon_b})} \\ &= P\left(-\sqrt{\epsilon_b}|H_1\right) = P\left(+\sqrt{\epsilon_b}|H_1\right) = Q\left(\sqrt{\tfrac{2\gamma_s}{1+\gamma_p}}\right). \end{aligned} \tag{26}$$

Similarly, assume that out of the x transmitted symbols, q_1 symbols are $-\sqrt{\epsilon_b}$ and g_1 of the q_1 symbols are incorrectly decoded as $+\sqrt{\epsilon_b}$, and that k_1 symbols out of the $x - q_1$ transmitted $+\sqrt{\epsilon_b}$ are incorrectly decoded as $-\sqrt{\epsilon_b}$. Thus, for a duration of $(g_1 + k_1)t_s$, the secondary signal is not removed from the received secondary frame, whilst for a duration of $(x - g_1 - k_1)t_s$, the secondary signal is correctly decoded and completely removed. Thus, when PU is present, one has the conditional probability of occurring for this case as

$$\begin{aligned} p(x, q_1, g_1, k_1|H_1) &= \left(P_{(-\sqrt{\epsilon_b})}B_{H_1}\right)^{g_1} \\ &\left(P_{(-\sqrt{\epsilon_b})}\left(1 - B_{H_1}\right)\right)^{q_1 - g_1}\left(P_{(+\sqrt{\epsilon_b})}B_{H_1}\right)^{k_1} \\ &\left(P_{(+\sqrt{\epsilon_b})}\left(1 - B_{H_1}\right)\right)^{x - q_1 - k_1}. \end{aligned} \tag{27}$$

B. Spectrum sensing

After the SU signal is decoded and deducted from the received secondary frame, the recovered signal is used for spectrum sensing. When the decoding error occurs such that the SU signal is not removed from the received secondary frame, the signal used for spectrum sensing is different from those of the conventional model and the ideal case of the new model. In this case, the decision variable or the received signal energy for binary hypothesis test becomes

$$y_{new(n)} = \begin{cases} \sum_{j=1}^{g_0}\left(-2\sqrt{\epsilon_b} + w_j\right)^2 + \sum_{j=g_0+1}^{k_0+g_0}\left(+2\sqrt{\epsilon_b}\right. \\ \left. + w_j\right)^2 + \sum_{j=g_0+k_0+1}^{Tf_s} w_j^2, & H_0, \\ \sum_{j=1}^{g_1}\left(s_{p,j} - 2\sqrt{\epsilon_b} + w_j\right)^2 + \sum_{j=g_1+1}^{k_1+g_1}\left(s_{p,j} + \right. \\ \left. 2\sqrt{\epsilon_b} + w_j\right)^2 + \sum_{j=g_1+k_1+1}^{Tf_s}\left(s_{p,j} + w_j\right)^2, & H_1. \end{cases} \tag{28}$$

Using the Gaussian approximation based on the central limit theorem, the mean and variance of the decision variable in (28) under hypothesis H_0 and H_1 can be derived as

$$\begin{cases} m_{H_0} = Tf_s + \dfrac{4\gamma_s}{x}(g_0 + k_0)Tf_s \\ \sigma^2_{H_0} = 2x + \dfrac{16\gamma_s}{x}(g_0 + k_0)Tf_s \end{cases} \tag{29}$$

and

$$\begin{cases} m_{H_1} = Tf_s(1 + \gamma_p) + \dfrac{4\gamma_s}{x}(g_1 + k_1)Tf_s \\ \sigma^2_{H_1} = 2x + 4\gamma_p Tf_s + \dfrac{16\gamma_s}{x}(g_1 + k_1)Tf_s \end{cases} \tag{30}$$

respectively. The conditional probability of detection for (28) can be derived as

$$P_{d_{newED}(n)}(T, q_1, g_1, k_1) = \frac{1}{2}erfc\left(\frac{\eta_{new_{ED}(n)} - m_{H_1}}{\sqrt{2\sigma^2_{H_1}}}\right) \tag{31}$$

where $\eta_{new_{ED}(n)}$ is the decision threshold for the new model with realistic decoding errors. The conditional probability of false alarm for (28) can be derived as

$$P_{f_{newED}(n)}(T, q_0, g_0, k_0) = \frac{1}{2}erfc\left(\frac{\eta_{new_{ED}(n)} - m_{H_0}}{\sqrt{2\sigma^2_{H_0}}}\right). \tag{32}$$

The unconditional results are given by

$$\begin{aligned} \overline{P_{d_{newED}(n)}}(T) &= \sum_{q_1=0}^{x}\sum_{g_1=0}^{q_1}\sum_{k_1=0}^{x-q_1}\binom{x}{q_1}\binom{q_1}{g_1}\binom{x-q_1}{k_1} \\ &\cdot\frac{\left(p(x, q_1, g_1, k_1|H_1)P_{d_{newED}(n)}(T, q_1, g_1, k_1)\right)}{\sum_{q_1=0}^{x}\sum_{g_1=0}^{q_1}\sum_{k_1=0}^{x-q_1}\binom{x}{q_1}\binom{q_1}{g_1}\binom{x-q_1}{k_1}p(x, q_1, g_1, k_1|H_1)} \end{aligned} \tag{33}$$

and

$$\begin{aligned} \overline{P_{f_{newED}(n)}}(T) &= \sum_{q_0=0}^{x}\sum_{g_0=0}^{q_0}\sum_{k_0=0}^{x-q_0}\binom{x}{q_0}\binom{q_0}{g_0}\binom{x-q_0}{k} \\ &\cdot\frac{\left(p(x, q_0, g_0, k_0|H_0)P_{f_{newED}(n)}(T, q_0, g_0, k_0)\right)}{\sum_{q_0=0}^{x}\sum_{g_0=0}^{q_0}\sum_{k_0=0}^{x-q_0}\binom{x}{q_0}\binom{q_0}{g_0}\binom{x-q_0}{k}p(x, q_0, g_0, k_0|H_0)}. \end{aligned} \tag{34}$$

In our paper, (33) is used in the Neyman-Pearson rule to determine the detection threshold without q_1, g_1 and k_1 so that the PU is protected by guaranteeing the average detection probability, because in practice the values of q_1, g_1 and k_1 are usually unknown and thus, the conditional probability of detection in (31) is averaged over (27) to remove them and the PU can't be protected against the instantaneous detection probability that requires q_1, g_1 and k_1. The unconditional results obtained after averaging are independent of q_1, g_1 and k_1. Moreover, obtaining threshold by using average and instantaneous probabilities give almost identical performances, as can be seen from the second paragraph in the right column of Page 1067 in [6].

C. Achievable throughput for data transmission

After spectrum sensing, the whole following frame can be used for data transmission if the sensing result favors the absence of the PU. The probability that the n^{th} frame is idle and is used for SU data transmission due to correct spectrum sensing at the $(n-1)^{th}$ frame can be derived as

$$\begin{aligned}
&P_{H_{0_{newED}}(n)} = P_{H_{0new}(n-1)}\big(1-p_{\lambda(n)}\big)\\
&\sum_{q_0=0}^{x}\sum_{g_0=0}^{q_0}\sum_{k_0=0}^{x-q_0}\binom{x}{q_0}\binom{q_0}{g_0}\binom{x-q_0}{k_0}\\
&\cdot\left(p(x,q_0,g_0,k_0|H_0)\Big(1-P_{f_{newED}(n)}(T,q_0,g_0,k_0)\Big)\right)\\
&+P_{H_{1_{new}}(n-1)p_{\lambda(n)}}\sum_{q_1=0}^{x}\sum_{g_1=0}^{q_1}\sum_{k_1=0}^{x-q_1}\binom{x}{q_1}\binom{q_1}{g_1}\binom{x-q_1}{k_1}\\
&\cdot\left(p(x,q_1,g_1,k_1|H_1)\Big(1-P_{d_{newED}(n)}(T,q_1,g_1,k_1)\Big)\right)
\end{aligned} \tag{35}$$

and the probability that the n^{th} frame is busy but is still used for data transmission due to mis-detection at the $(n-1)^{th}$ frame can be derived as

$$\begin{aligned}
&P_{H_{1_{newED}}(n)} = P_{H_{0_{new}}(n-1)p_{\lambda(n)}}\\
&\sum_{q_0=0}^{x}\sum_{g_0=0}^{q_0}\sum_{k_0=0}^{x-q_0}\binom{x}{q_0}\binom{q_0}{g_0}\binom{x-q_0}{k_0}\\
&\cdot\left(p(x,q_0,g_0,k_0|H_0)\Big(1-P_{f_{newED}(n)}(T,q_0,g_0,k_0)\Big)\right)\\
&+P_{H_{1_{newED}}(n-1)}\big(1-p_{\lambda(n)}\big)\\
&\sum_{q_1=0}^{x}\sum_{g_1=0}^{q_1}\sum_{k_1=0}^{x-q_1}\binom{x}{q_1}\binom{q_1}{g_1}\binom{x-q_1}{k_1}\\
&\cdot\left(p(x,q_1,g_1,k_1|H_1)\Big(1-P_{d_{newED}(n)}(T,q_1,g_1,k_1)\Big)\right).
\end{aligned} \tag{36}$$

Using (35) and (36), the total achievable throughput of the N frames when energy detection is used in the new model can be derived as

$$R_{new_{ED}} = \sum_{n=1}^{N}\Big(P_{H_{0_{newED}}(n)}C_0 + P_{H_{1_{newED}}(n)}C_1\Big). \tag{37}$$

Next, we derive results for feature detection. When the SU symbols are independent, the covariance matrix of the SU signal is diagonal. When maximum-eigenvalue detection is applied, the conditional probability of detection and the conditional probability of false alarm can be derived as

$$\begin{aligned}
&P_{d_{newME}(n)}(T) =\\
&\qquad 1-TW_1\left(\frac{\eta_{new_{ME}(n)}Tf_s - \frac{Tf_s\vartheta_{max}}{\sigma_w^2+\sigma_{s_s}^2} - \mu_{new}}{\upsilon_{new}}\right)
\end{aligned} \tag{38}$$

and

$$P_{f_{newME}(n)}(T) = 1-TW_1\left(\frac{\eta_{new_{ME}(n)}Tf_s - \mu_{new}}{\upsilon_{new}}\right) \tag{39}$$

respectively, where $\eta_{new_{ME}(n)}$ is the decision threshold for the new model when maximum-eigenvalue detection is applied, $\mu_{new} = (\sqrt{Tf_s-1}+\sqrt{L})^2$, $\upsilon_{new} = (\sqrt{Tf_s-1}+\sqrt{L})(\frac{1}{\sqrt{Tf_s-1}}+\frac{1}{\sqrt{L}})$, $\sigma_{s_s}^2 = \epsilon_b$, and ϵ_b is the secondary bit energy defined as before.

When the covariance-based detection is applied, the probability of detection and the probability of false alarm can be derived as

$$\begin{aligned}
&P_{d_{newCOV}(n)}(T) =\\
&1-Q\left(\frac{\frac{1}{\eta_{new_{COV}(n)}}+\frac{\alpha_L\gamma_p}{\eta_{new_{COV}(n)}\left(\gamma_p+\frac{k_1+g_1}{Tf_s}4\gamma_s+1\right)}-1}{\sqrt{\frac{2}{Tf_s}}}\right)
\end{aligned} \tag{40}$$

and

$$\begin{aligned}
&P_{f_{newCOV}(n)}(T) =\\
&\qquad 1-Q\left(\frac{\frac{1}{\eta_{new_{COV}(n)}}\left(1+(L-1)\sqrt{\frac{2}{Tf_s\pi}}\right)-1}{\sqrt{\frac{2}{Tf_s}}}\right)
\end{aligned} \tag{41}$$

where $\eta_{new_{COV}(n)}$ is the decision threshold for the new model when covariance-based detection is applied and other symbols are defined as before.

The achievable throughput of the new model when feature detection is used for spectrum sensing can then be derived by using the same method as that of (33) - (37) but replacing the probability of detection and the probability of false alarm with (38) and (39) for maximum-eigenvalue detection or (40) and (41) for covariance-based detection. When other types of modulation schemes are used for the SU signal, such as quadrature phase shift keying (QPSK), the probability of error will be different. However, the performance of the new model with decoding errors can be analyzed in a similar way to that in (28) - (41).

D. Effect of fading

In the above analysis, it is assumed that the SU is only corrupted by AWGN. In practice, wireless signals may experience fading and consequently it affects the system performance. In this section, the effect of fading is analyzed.

Assume that the channel from the PU transmitter to the SU receiver suffers from Rayleigh fading such that the fading coefficient h_p is Rayleigh distributed and the received PU SNR is chi-square distributed with parameter $\overline{\gamma_{pu}}$. This is a reasonable assumption as the PU is normally far away from the SU receiver without line-of-sight. Further, assume that the secondary signal also suffers from Rayleigh fading with fading

coefficient h_s and parameter $\overline{\gamma_{su}}$. The received signal at the secondary receiver becomes

$$Y_{newF,j}(n) = ah_p s_{p,j} + h_s s_{s,j} + w_j \tag{42}$$

where the notations are defined as before.

When the PU is absent, the received signal in (42) contains only the corrupted SU signal and noise. As h_s is random, the symbol error rate in (24) is averaged to give [22]

$$B_{H_0F} = \int_0^\infty B_{H_0} \frac{1}{\overline{\gamma_{su}}} e^{\frac{-\gamma_{su}}{\overline{\gamma_{su}}}} d\gamma_{su} \tag{43}$$

where $\gamma_{su} = h_s^2 \gamma_s$, $\overline{\gamma_{su}} = E(h_s^2)\gamma_s$, and $E(h_s^2)$ is the average fading power of SU.

When the PU is present, taking into consideration the effect of fading experienced by both the PU signal and the SU signal, the symbol error rate in (26) is averaged to give

$$B_{H_1F} = \int_0^\infty \int_0^\infty B_{H_1} \frac{1}{\overline{\gamma_{su}}} e^{\frac{-\gamma_{su}}{\overline{\gamma_{su}}}} \frac{1}{\overline{\gamma_{pu}}} e^{\frac{-\gamma_{pu}}{\overline{\gamma_{pu}}}} d\gamma_{su}\gamma_{pu} \tag{44}$$

where $\gamma_{pu} = h_p^2 \gamma_p$, $\overline{\gamma_{pu}} = E(h_p^2)\gamma_p$, and $E(h_p^2)$ is the average fading power of PU. The probability of occurring in (25) and (27) can then be re-derived by using the new symbol error rates in (43) and (44).

The conditional probability of detection in (31) can be derived as

$$\begin{aligned} P_{d_{new}F(n)}(T, q_1, g_1, k_1) = \int_0^\infty \int_0^\infty \frac{1}{\overline{\gamma_{su}}} e^{\frac{-\gamma_{su}}{\overline{\gamma_{su}}}} \\ \cdot \frac{1}{\overline{\gamma_{pu}}} e^{\frac{-\gamma_{pu}}{\overline{\gamma_{pu}}}} P_{d_{new}ED(n)}(T, q_1, g_1, k_1)\, d\gamma_{su} d\gamma_{pu}. \end{aligned} \tag{45}$$

The unconditional probability of detection can then be obtained by averaging (45) over the probability of occurring to remove the dependency on the values of q_1, g_1 and k_1.

The conditional probability of false alarm in (32) can also be derived as

$$\begin{aligned} P_{f_{new}F(n)}(T, q_0, g_0, k_0) &= \int_0^\infty P_{f_{new}ED(n)}(T, q_0, g_0, k_0) \\ &\quad \cdot \frac{1}{\overline{\gamma_{su}}} e^{\frac{-\gamma_{su}}{\overline{\gamma_{su}}}} d\gamma_{su}. \end{aligned} \tag{46}$$

The unconditional probability of false alarm is then be obtained by averaging (46) over the probability of occurring to remove the dependency on the values of q_0, g_0 and k_0.

When the effect of fading channel is considered, the achievable throughput of the SU transmission is also affected. When the PU is absent, the average channel capacity C_0 becomes

$$C_{0F} = \int_0^\infty C_0 \frac{1}{\overline{\gamma_{su}}} e^{\frac{-\gamma_{su}}{\overline{\gamma_{su}}}}\ \gamma_{su} \tag{47}$$

and when the PU is present, the average channel capacity C_1 becomes

$$C_{1F} = \int_0^\infty \int_0^\infty C_1 \frac{1}{\overline{\gamma_{su}}} e^{\frac{-\gamma_{su}}{\overline{\gamma_{su}}}} \frac{1}{\overline{\gamma_{pu}}} e^{\frac{-\gamma_{pu}}{\overline{\gamma_{pu}}}} d\gamma_{su} d\gamma_{pu}. \tag{48}$$

The total achievable throughput can then be derived by using (47) and (48). In the above, perfect CSI is assumed in detection and then used in sensing.

E. Coded Signals

In the above, the SU signal is assumed to be uncoded. In practice, error control codes (ECC) can be applied to reduce errors at the receiver [22].

Consider Golay (23, 12) coded BPSK signal for the SU signal. Golay (23, 12) is a binary linear code with minimum distance of $d_{min} = 7$ and can correct up to three errors in a block of 23 elements [22]. When hard decision decoding is applied at the secondary receiver, the probabilities of decoding error in (24) and (26) become

$$B_{H_0Golay} = \sum_{z=4}^{23} \binom{23}{z} B_{H_0}^z \left(1 - B_{H_0}\right)^{23-z} \tag{49}$$

and

$$B_{H_1Golay} = \sum_{z=4}^{23} \binom{23}{z} B_{H_1}^z \left(1 - B_{H_1}\right)^{23-z} \tag{50}$$

respectively.

Alternatively, consider Hamming (7, 4) coded BPSK signal for the SU signal. Hamming (7, 4) is a linear block code with minimum distance of $d_{min} = 3$ and can correct only one error in a block of 7 elements [22]. The probabilities of decoding error in (24) and (26) become

$$B_{H_0Ham} = \sum_{z=2}^{7} \binom{7}{z} B_{H_0}^z \left(1 - B_{H_0}\right)^{7-z} \tag{51}$$

and

$$B_{H_1Ham} = \sum_{z=2}^{7} \binom{7}{z} B_{H_1}^z \left(1 - B_{H_1}\right)^{7-z} \tag{52}$$

respectively.

Substituting (49) and (50) or (51) and (52) for (24) and (26) for the Golay (23, 12) coded secondary signal and the Hamming (7, 4) coded secondary signal, respectively, the performances of spectrum sensing and data transmission can be analyzed in a similar way to before.

IV. Numerical Results and Discussion

In this section, the performance of the new model with decoding error is examined and compared with the performances of the conventional model and the ideal case of the new model by providing numerical examples. In the examination, $t_s = 5\ \mu s$, $T = 80\ \mu s$ and $f_s = 1\ MHz$. The receiver operating characteristics (ROC) for spectrum sensing and the achievable throughput for data transmission in different models are studied. Neyman-Pearson rule is applied to obtain the decision threshold for spectrum sensing by setting the target probability of detection to 0.9. Note that in the new model with decoding errors, the unconditional probability of detection in (33) is used when applying the Neyman-Pearson rule, rather than the conditional probability in (31), as the former does not require knowledge of g_1, q_1 and k_1. Even when g_1, q_1 and k_1 were known, their difference is negligible [6].

Fig. 1 shows the ROC curves of different models of the n^{th} frame when energy detection is applied for spectrum sensing and different coding schemes are applied for the SU signal. In this figure, γ_p =-5 dB and $\gamma_s = 3\ dB$. Several observations

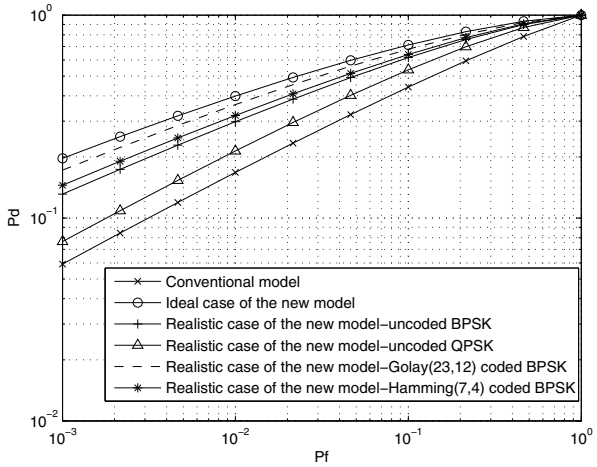

Fig. 1. Comparison of the ROC curves for different models when energy detection is applied with γ_p = -5 dB and γ_s = 3 dB for the n^{th} frame.

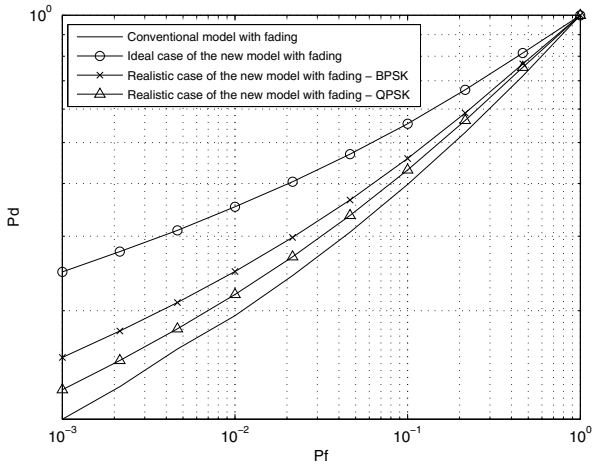

Fig. 2. Comparison of the ROC curves for different models when fading is taken into consderation with γ_p = -5 dB and γ_s = 3 dB for the n^{th} frame.

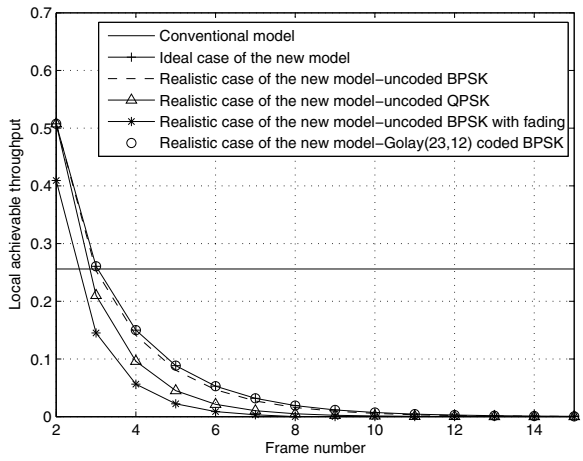

Fig. 3. The individual achievable throughputs for different frames in different models when energy detection is applied with γ_p = -5 dB and γ_s = 0 dB.

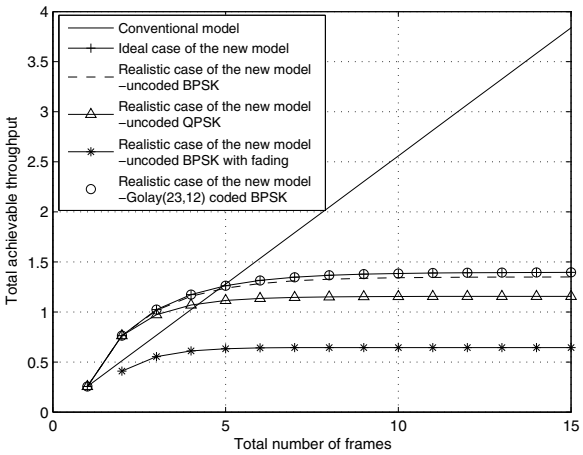

Fig. 4. The total achievable throughputs for different models when energy detection is applied with γ_p = -5 dB and γ_s = 0 dB.

can be made from Fig. 1. First, the new model takes advantage of the longer sensing period and thus, has a better sensing performance. For the same target probability of false alarm, it has higher probability of detection. Second, the ideal case analyzed in [8] provides an upper bound of the sensing performance by ignoring the decoding errors. As well, the sensing accuracy is lower for uncoded QPSK than for uncoded BPSK, because QPSK has a larger probability of error and hence, more residual SU signal in the sample. Finally, when ECC is applied, the sensing performance is improved as the decreased BER results in less residual secondary signal in the samples. Fig. 2 examines the effect of fading on the ROC curves for different models of the n^{th} frame. Energy detection is applied for spectrum sensing and the SU signal is uncoded. One sees that, when the effect of fading is considered, similar observations to those from Fig. 1 can be made.

Fig. 3 examines the individual achievable throughputs for different frames in different models. Energy detection is applied for spectrum sensing. First, as the frame index n increases, the individual achievable throughput of the conventional model remains the same, while in the new model, the individual achievable throughput decreases and approaches zero. This is because after the initial idle status of the licensed channel is acquired, the probability that the n^{th} frame can be used for data transmission depends on the sensing results of the previous $n-1$ frames in the new model. Since the probability that all the previous $n-1$ frames have mis-detection or false alarm decreases when n increases, the secondary transmission opportunity also decreases leading to smaller achievable throughput. Second, the sensing performance degrades when the decoding error occurs. Thus, in the realistic case of the new model, the decrease of the individual achievable throughput is faster than that in the ideal case. The speed of decreasing can be reduced by using ECC. Moreover, for uncoded QPSK, the decrease in the achievable throughput is more significant than that for uncoded BPSK. When fading is considered, the achievable throughput is significantly reduced compared with the no-fading cases.

Fig. 4 examines the total achievable throughput of the N consecutive frames in different models. In this figure, the

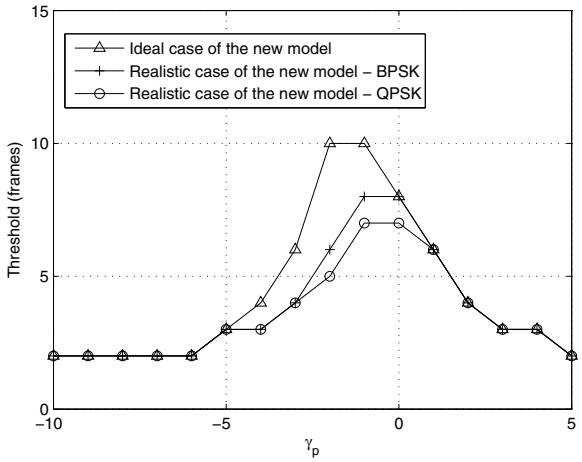

Fig. 5. The effect of the primary user SNR on the threshold of the new model when energy detection is applied with γ_s = 0 dB.

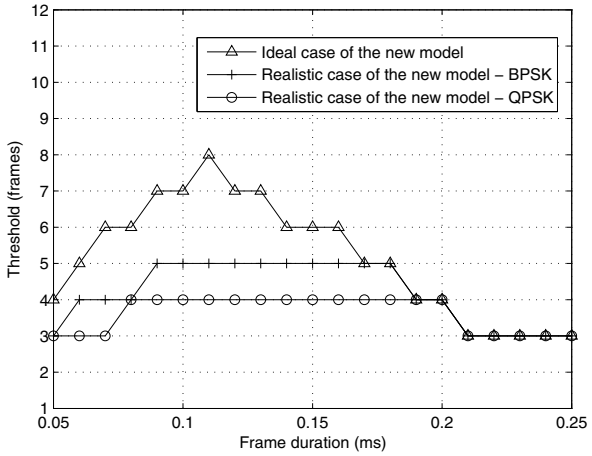

Fig. 6. The effect of the frame duration on the threshold of the new model when energy detection is applied with γ_p = -3 dB and γ_s = 0 dB.

energy detection is used and the PU's mean channel holding time is $10T$. Although the total achievable throughputs for all the models increase with the number of frames N, the total achievable throughput in the conventional model increases linearly, while it approaches a limit in the new model. Define the number of frames for which the new and conventional models have the same throughput as a threshold. When the total number of frames is beyond this threshold, the new model loses its throughput advantage even when the whole frame is used for data transmission. The existence of this threshold is caused by the dependence of the secondary transmission opportunity on the sensing results of the previous frames, as well as the accumulation of the decoding errors over frames. When ECC is applied, the system performance becomes almost the same as that of the ideal case due to the decrease in BER. When fading is considered, there is no advantage for the new model in this case. Thus, fading degrades the performance of the new model while coding improves it, as expected.

Fig. 5 investigates the effect of the received PU SNR on the threshold value of the number of transmitted secondary

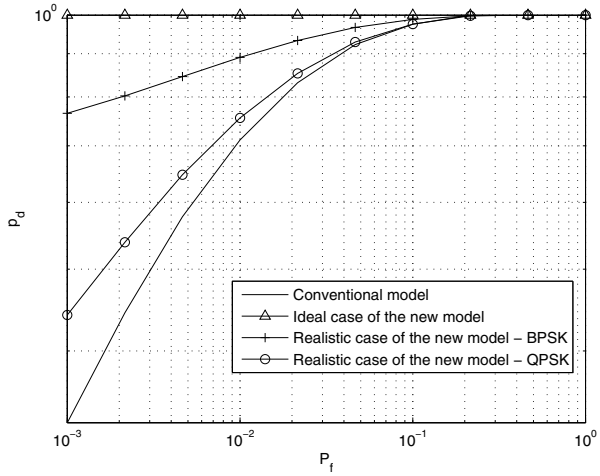

Fig. 7. Comparison of the ROC curves for different models when maximum-eigenvalue detection is applied with γ_p = -10 dB and γ_s = 0 dB.

frames in the new model. When γ_p increases at small values, the new model takes advantage of a longer sensing duration to capture more secondary transmission opportunities and hence, the threshold of the new model increases. After γ_p reaches certain values, about -1 dB in this case, the sensing result is accurate enough such that the new model suffers more from the PU interference and therefore the threshold decreases. Moreover, when decoding error occurs, the threshold of the new model decreases further.

Fig. 6 investigate the effect of the frame duration T on the threshold of the new model. As can be seen from Fig. 6, there exists an optimal value of T where the threshold of the new model or the advantage of the new model are maximized. This can be explained as follows. At small values of T, the advantage of the new model in spectrum sensing increases as T increases. The threshold of the new model therefore increases due to the increased secondary transmission opportunity. When the value of T increases further, as shown in [6], the fraction of the frame used for transmission becomes larger for the conventional model, and the sensing period in the conventional model is significantly smaller than the transmission period. In this case, the conventional model will be similar to the new model. As well, since the channel holding time parameter λ is fixed, the increase of the frame duration leads to more status changes of the PU. This increases the probability of decoding error and hence, degrades the performance.

Fig. 7 compares the ROC curves in different models when maximum-eigenvalue detection is applied for spectrum sensing. In this figure, the smoothing factor is set at 5 and ρ is set at 0.5. As can be seen, maximum-eigenvalue detection has much better performance than energy detection in Fig. 1. Also, the sensing performance difference between the new model and the conventional model is larger. Fig. 8 investigates the individual achievable throughput versus the frame index for different models when maximum-eigenvalue detection is applied for spectrum sensing. As can be seen, due to the improvement in the sensing performance as demonstrated in Fig. 7, the individual achievable throughputs for both the

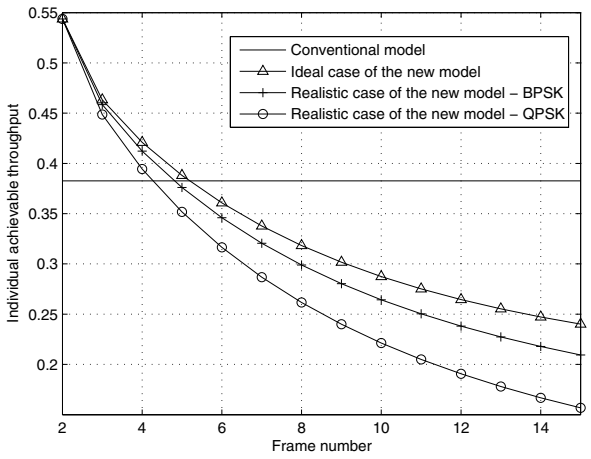

Fig. 8. The individual achievable throughputs for different models when maximum-eigenvalue detection is applied with γ_p = -10 dB and γ_s = 0 dB.

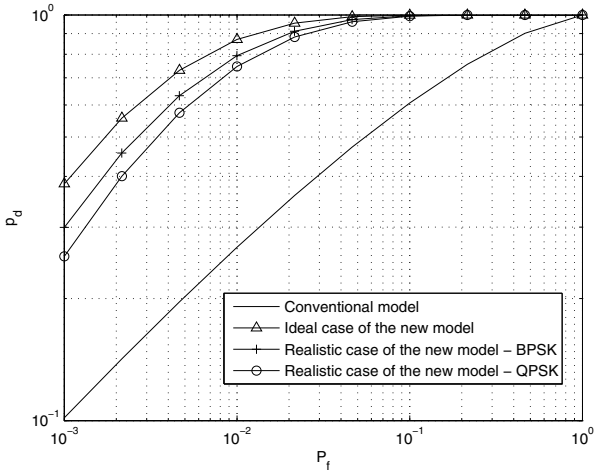

Fig. 10. Comparison of ROC curves for different models when covariance-based detection is applied with γ_p = -5 dB and γ_s = 0 dB.

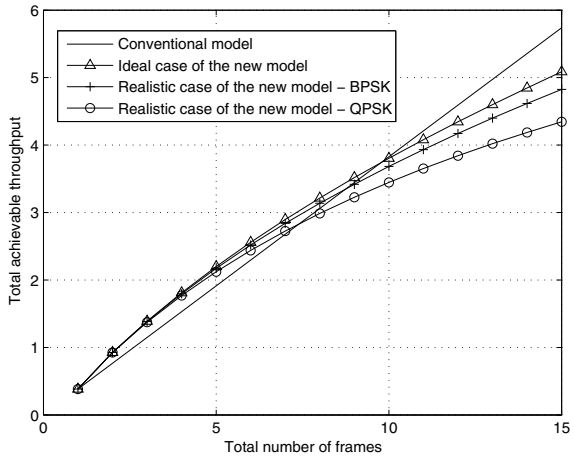

Fig. 9. The total achievable throughputs for different models when maximum-eigenvalue detection is applied, where γ_p = -10 dB and γ_s = 0 dB.

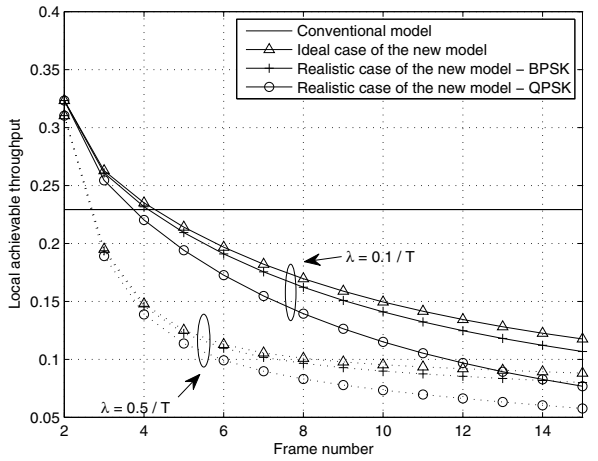

Fig. 11. The individual achievable throughputs for different models when covariance-based detection is applied with γ_p = -5 dB and γ_s = 0 dB. Solid lines are results with mean channel holding time $\frac{1}{\lambda}$ = 10T and dotted lines are results with $\frac{1}{\lambda}$ = 2T.

conventional model and the new model become larger compared with Fig. 3. Again, the individual achievable throughput decreases as the frame index increases. However, the speed of decrease is smaller than energy detection in Fig. 3. Fig. 9 examines the total achievable throughput of the N consecutive frames for different models when maximum-eigenvalue detection is applied for spectrum sensing. Again, in the conventional model, the total achievable throughput increases linearly as the total number of frames increases. The total achievable throughput of the new model also increases with N. This agrees with the previous finding in Fig. 4. However, it can be noted that the rate of increase for the new model in this case is much higher than that in Fig. 4. In other words, the threshold value using maximum-eigenvalue detection is much larger than that using energy detection. This is due to the improvement in the sensing performance by using maximum-eigenvalue detection.

Fig. 10 compares the ROC curves for different models when covariance-based detection is applied for spectrum sensing. As can be seen, when covariance-based detection is applied, the performance of spectrum sensing is better than energy detection presented in Fig. 1, while it is worse than that of maximum-eigenvalue detection presented in Fig. 7. This agrees with the findings in [20]. Again, the new model takes advantage of the longer sensing period and has a better performance than the conventional model. Fig. 11 compares the individual achievable throughputs for different models when covariance-based detection is used for spectrum sensing. Compared with Fig. 3 and Fig. 8, it can be noticed that, the local achievable throughput performance using covariance-based detection falls between those for energy detection and maximum-eigenvalue detection. This also agrees with the findings from Fig. 10. Also, Fig. 11 examines the effect of different mean channel holding time. When the mean channel holding time $\frac{1}{\lambda}$ decreases from $10T$ to $2T$, the performance of the new model degrades, as a result of the increased PU traffic. Similar findings can also be made for energy detection

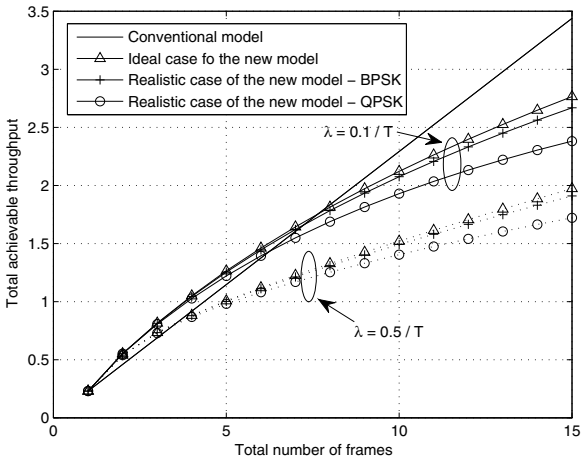

Fig. 12. The total achievable throughputs for different models when covariance-based detection is used with γ_p = -5 dB and γ_s = 0 dB. Solid lines are results with mean channel holding time $\frac{1}{\lambda} = 10T$ and dotted lines are results with $\frac{1}{\lambda} = 2T$.

and maximum-eigenvalue detection. Fig. 12 provides the total achievable throughput for different models when covariance-based detection is applied for spectrum sensing. In this case, the threshold value of the new model is 8 frames for the ideal case of the new model, 7 frames for the new model with BPSK and 6 frames for the new model with QPSK. These figures are larger than those of energy detection but smaller than those of maximum-eigenvalue detection. When the mean channel holding time is decreased, the system performance degrades and the threshold value of the new model is reduced to 3 frames. The effects of fading and coding can be examined similarly for feature detection but they are not presented here due to the length restriction.

V. Conclusion

The realistic performance of the new model proposed in [8] has been analyzed and compared with that of the conventional model and the ideal performance. It has been shown that, when the decoding error is taken into account, the system performance is degraded. Moreover, the new model has a threshold below which it outperforms the conventional model with multiple consecutive frames. This threshold depends on the spectrum sensing technique and the secondary signal modulation scheme. The new model is more suitable for feature detection than for energy detection. Our results have given detailed guidlines to the choices of these parameters for best performance in practice.

References

[1] J. Tang and S. Lambotharan, "Beamforming and temporal power optimisation for an overlay cognitive radio relay network," *IET Signal Process.*, vol. 5, no. 6, pp. 582–588, Sep. 2011.

[2] I. Krikidis, J. N. Laneman, J. Thompson, and S. McLaughlin, "Stability analysis for cognitive radio with cooperative enhancements," in *Proc. 2009 IEEE Information Theory Workshop on Networking and Information Theory*, pp. 286–290.

[3] Rui Zhang, "On active learning and supervised transmission of spectrum sharing based cognitive radios by exploiting hidden primary radio feedback," *IEEE Trans. Commun.*, vol. 58, no. 10, pp. 2960–2970, Oct. 2010.

[4] T. Yucek and H. Arslan, "A survey of spectrum sensing algorithms for cognitive radio applications," *IEEE Commun. Surveys and Tutorials*, vol. 11, no. 1, pp. 116–130, First Quarter 2009.

[5] L. Berlemann and S. Mangold, *Cognitive Radio and Dynamic Spectrum Access*. John Wiley & Sons, 2009.

[6] L. Tang, Y. Chen, E. L. Hines, and M. -S. Alouini, "Effect of primary user traffic on sensing-throughput tradeoff for cognitive tadios," *IEEE Trans. Wireless Commun.*, vol. 10, no. 4, pp. 1063–1068, Apr. 2011.

[7] A. Hoang, Y.-C. Liang, and Y. Zeng, " Adaptive joint scheduling of spectrum sensing and data transmission in cognitive radio networks," *IEEE Trans. Commun.*, vol. 58, no. 1, pp. 235–246, Jan. 2010.

[8] S. Stotas and A. Nallanathan, "Overcoming the sensing-throughput tradeoff in cognitive radio networks," in *2010 IEEE Int. Conf. on Commun.*

[9] J. C. Bellamy, *Digital Telephony*, 3rd edition. John Wiley & Sons. Inc., 2000.

[10] A. Ghasemi and E. S. Sousa, "Optimization of spectrum sensing for opportunistic spectrum access in cognitive radio networks," in *Proc. 2007 IEEE Consumer Commun. and Networking Conf.*, pp. 1022–1026.

[11] C. Jedrzycki and V. C. M. Leung, "Probability distribution of channel holding time in cellular telephony systems," in *Proc. 1996 IEEE Vehicular Technology Conf. – Spring*, vol. 1, pp. 247–251.

[12] F. Barcelo and J. Jordan, "Channel holding time distribution in cellular telephony," *IEEE Trans. Veh. Technol.,*, vol. 49, no. 5, pp. 1615–1652, Sep. 2000.

[13] X. Li and S. A. Zekavat, "Traffic pattern prediction and performance investigation for cognitive radio systems," in *Proc. 2008 IEEE Wireless Commun. and Networking Conf.*, pp. 894–899.

[14] M. Alwakeel, "Deriving call holding time distribution in cellular network from empirical data," *Int. J. Computer Science and Network Security*, vol. 9, no. 11, Nov. 2009.

[15] Y. Fang, I. Chlamtac, and Y.-B. Lin, "Modeling PCS networks under general call holding time and cell residence time distributions," *IEEE Trans. Networking*, vol. 5, no. 6, Dec. 1997.

[16] J. Ma, X. Zhou, and G. Y. Li, "Probability-based periodic spectrum sensing during secondary communication," *IEEE Trans. Commun.*, vol. 58, no. 4, pp. 1291–1301, Apr. 2010.

[17] H. Urkowitz, "Energy detection of unknown deterministic signals," *Proc. IEEE*, vol. 44, no. 4, pp. 523–531, Apr. 1967.

[18] Y. Zeng and Y. -C. Liang, "Spectrum-sensing algorithms for cognitive radio based on statistical covariances," *IEEE Trans. Veh. Technol.*, vol. 58, no. 4, pp. 1804–1815, May 2009.

[19] Y. Zeng, C. L. Koh, and Y.-C. Liang, "Maximum eigenvalue detection: theory and application," in *Proc. 2008 IEEE International Conf. on Commun.*, pp. 4160–4164.

[20] Y. Chen, C. Wang, and B. Zhao, "Performance comparison of feature-based detectors for spectrum sensing in the presence of primary user traffic," *IEEE Signal Process. Lett.*, vol. 18, no. 5, pp. 291–294, May 2011.

[21] T. Wang, Y. Chen, E. L. Hines, and B. Zhao, "Analysis of effect of primary user traffic on spectrum sensing performance," in *Proc. 2009 Int. Conf. on Commun. and Networking in China*, pp. 1–5.

[22] J. G. Proakis, *Digital Communications*, 3rd edition. McGraw-Hill, Inc., 1995.

Liang Tang (S'12) received her B.Eng degree in Electronic and Electrical Engineering from the University College London in 2007 and her M.Sc degree in Advanced Electronics from University of Warwick in 2008. She is currently a Ph. D student in the University of Warwick. Her research interest is cognitive radio.

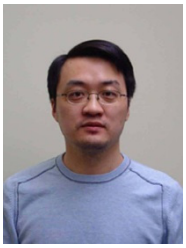

Yunfei Chen (S'02-M'06-SM'10) received his B.E. and M.E. degrees in electronics engineering from Shanghai Jiaotong University, Shanghai, P.R.China, in 1998 and 2001, respectively. He received his Ph.D. degree from the University of Alberta in 2006. He is currently working as an Associate Professor at the University of Warwick, U.K. His research interests include cognitive radio, ultra-wide bandwidth and multiple-input-multiple-output systems.

Arumugam Nallanathan (S'97-M'00-SM'05) is the Head of Graduate Studies in the School of Natural and Mathematical Sciences and a Reader in Communications at King's College London, London, U.K. From August 2000 to December 2007, he was an Assistant Professor in the Department of Electrical and Computer Engineering at the National University of Singapore, Singapore. His research interests include smart grid, cognitive radio, and relay networks. He has authored nearly 200 journal and conference papers. He is an Editor for IEEE TRANSACTIONS ON COMMUNICATIONS, IEEE TRANSACTIONS ON VEHICULAR TECHNOLOGY, IEEE WIRELESS COMMUNICATIONS LETTERS, and IEEE SIGNAL PROCESSING LETTERS. He served as an Editor for IEEE TRANSACTIONS ON WIRELESS COMMUNICATIONS (2006-2011) and as a Guest Editor for the *EURASIP Journal of Wireless Communications and Networking* Special Issue on UWB Communication Systems-Technology and Applications. He served as the General Track Chair for the Spring 2008 IEEE Vehicular Technology Conference (VTC'2008) and Co-Chair for the 2008 IEEE Global Communications Conference (GLOBECOM'2008) Signal Processing for Communications Symposium, 2009 IEEE International Conference on Communications (ICC'2009) Wireless Communications Symposium, 2011 IEEE Global Communications Conference (GLOBECOM'2011) Signal Processing for Communications Symposium and the 2012 IEEE International Conference on Communications (ICC'2012) Signal Processing for Communications Symposium. He also served as the Technical Program Co-Chair for the 2011 IEEE International Conference on Ultra-Wideband (ICUWB'2011). He currently serves as 2013 IEEE Global Communications Conference (GLOBECOM'2013) Communications Theory Symposium. He is the Vice-Chair for the Signal Processing for Communication Electronics Technical Committee of the IEEE Communications Society. He was a co-recipient of the Best Paper Award presented at the 2007 IEEE International Conference on Ultra-Wideband.

Evor L. Hines joined Warwick University in 1984 and he is a Professor in the School of Engineering. He became a Fellow of the Higher Education Academy (FHEA) in 2000 and was awarded his DSc (Warwick) in 2007. He is a chartered Engineer and a Fellow of IET. His main research interest is concerned with Intelligent Systems (also known by other names such as Computational Intelligence and Soft Computing) and their applications. Most of his work have focused on Artificial Neural Networks, Genetic Algorithms, Fuzzy Logic, Neuro-Fuzzy Systems, and Genetic Programming. Typical application areas include intelligent sensors (e.g., electronic nose), medicine, non-destructive testing of, for example, composite materials, computer vision, telecommunications, amongst others. He has for example co-authored some 215 articles and supervised more 30 successful research students. He currently leads the School's Intelligent Systems Engineering Laboratory which he established in 1990. His work has been funded by numerous organizations including several EPRSC and EU and he acts as a referee for a range of journals.